ChemPubSoc Europe

DOI: 10.1002/cplu.201800534

CHEMPLUSCHEM Full Papers

Photocurrent Response and Progesterone Degradation by Employing WO_3 Films Modified with Platinum and Silver Nanoparticles

Maria Joseita dos Santos Costa,[a] Gilson dos Santos Costa,[a] Aline Estefany Brandão Lima,[a] Geraldo Eduardo da Luz Júnior,[a] Elson Longo,[b] Laécio Santos Cavalcante,*[a] and Reginaldo da Silva Santos[a]

The effect of silver (Ag^0) and platinum (Pt^0) metallic nanoparticles (NPs) on WO_3 film was investigated by studying the photocurrent response under polychromatic irradiation. The structural phase revealed by X-ray diffraction analysis indicates a monoclinic crystal nanostructure. WO_3, Ag^0/WO_3, and Pt^0/WO_3 electrodes were used to degrade 0.35 mg L^{-1} progesterone hormone in aqueous solution under polychromatic irradiation for 3h. The studies on degradation were investigated under electrochemically assisted heterogeneous photocatalysis (EHP) conditions. For photodegradation of progesterone, higher performance was achieved when WO_3 was functionalized and when the EHP configuration was adopted with bias at +0.7 V vs Ag/AgCl. This study reveals that incorporation of metallic NPs onto a semiconductor increases its efficiency, thereby preventing electron-hole recombination in the photocatalyst and photoelectrochemical limitations of WO_3 due to surface plasmon resonance and the trapping state. Therefore, efficient advances in the degradation of organic contaminants during water treatment can be realized.

Introduction

Over the last ten years, the population worldwide have increased drastically, the demand for industrialized products has grown. Among the industrialized products, we highlight a series of new synthetic compounds produced annually; these products are discarded indiscriminately in nature without any previous treatment. Most of these pollutants are organic compounds such as polymers, herbicides, pesticides, dyes, and drugs. Some pharmaceuticals drugs are typical pollutants that take a long time to degrade under natural condition and can be considered a major problem for human health.

Studies have shown that drugs are released directly or indirectly into rivers, lakes, and groundwater. Consequently, these drugs can return to the water supply system because are not removed by conventional water treatment methods.[1–3] Several forms of hormones (synthetic or natural) are widely used as oral contraceptives and in hormonal replacement therapy and treatment of gynecological disorders.[4] Among hormones, progesterone and estrogen are excreted in the highest concentrations, and they have been detected in aqueous environments.[3,5] Studies have shown that these hormones pose risks to male fish and other aquatic organisms, even at extremely low concentrations (~1 ng L^{-1}). The main problems caused by these hormones are decrease in fertility, feminization of male organisms, and hermaphroditism. Similar adverse effects are caused by these hormones in humans as well, and these aqueous pollutants can alter the endocrinal system and increase the risk of cancer.[6,7] The chemical structure of hormones imparts them excellent stability, and hence, they are dominant persistent pollutants.

Advanced oxidation processes (AOPs) have proved to be useful for degrading several organic pollutants.[8] On the whole, AOPs are associated with oxidation process caused by hydroxyl radicals (•OH), which have high oxidizing power and can promote the complete degradation of various pollutants.[9,10] Photocatalysis using semiconductor oxides can be considered an AOP methodology because •OH are formed on semiconductor surface upon irradiation with appropriated wavelength of the source light. Several recent studies explored the removal of a variety of organic and inorganic contaminants using semiconductor oxides. Photocatalysts are usually developed using materials in colloidal suspension or immobilized on different substrates. The main advantage of using an immobilized photocatalyst is that it can be recovered for reuse.

Photoelectrocatalytic technologies using semiconductors have received great attention owing to their potential and effectiveness in wastewater treatment.[11] However, rapid recombination of the photogenerated electrons/holes (e^-/h^+) is the major drawback for this methodology. Some strategies adopted to prevent charge recombination are combining different semiconductors (i.e., a composite), doping the catalyst with a

[a] M. Joseita dos Santos Costa, G. dos Santos Costa, Dr. A. Estefany Brandão Lima, Prof. Dr. G. Eduardo da Luz Júnior, Prof. Dr. L. Santos Cavalcante, Prof. Dr. R. da Silva Santos
Department of Chemistry
PPGQ-GERATEC
Universidade Estadual do Piauí
Rua: João Cabral, N. 2231, P.O. Box 381, Teresina PI 64002-150 (Brazil)
E-mail: laeciosc@gmail.com

[b] Dr. E. Longo
Department of Chemistry of Materials
CDMF-Universidade Estadual Paulista
P.O. Box 355, Araraquara, SP 14801-907 (Brazil)

Supporting information for this article is available on the WWW under https://doi.org/10.1002/cplu.201800534

metal or nonmetal, modifying the surface with metallic nanoparticles, and applying potential on supported semiconductor films.[12–14] The last methodology is termed electrochemically assisted heterogeneous photocatalysis (EHP). For EHP, a semiconductor should be immobilized on a conductive material to apply a bias potential. This process not only increases the efficiency and reduces costs, but also increases the rate of degradation of the recalcitrant pollutants.[15,16]

Several semiconductors have been investigated as candidate photocatalyst materials for degrading many organic pollutants. Among them, WO_3 is a typical *n*-type $5d^0$ transition metal oxide semiconductor[17] with an optical energy band gap (E_{BG}) ranging from 2.6 to 2.8 eV, which allows the use of visible light. Semiconductor photocatalytic reactions occur when the electrons are excited from the valence band (VB) to the conduction band (CB). In EHP with an *n*-type semiconductor, the photoexcited electrons can be collected by an external circuit, while holes move in direction to surface of the semiconductor, generating •OH radicals and other reactive species.[18,19] Recently, Mohite and co-workers[20] prepared a WO_3 film on conductive glass with different solution concentrations using the chemical spray pyrolysis technique and investigated its photocatalytic and photoelectrocatalytic performance in the degradation of Rhodamine-B under solar radiation.

WO_3 has many advantages such as good chemical stability in acid solution, easy synthesis, wide light absorption range, low cost, and toxicity.[21] In contrast, the photoelectrochemical performance of the WO_3 photoelectrode is limited owing to its rapid electron-hole charge recombination and photocorrosion in an alkaline medium.[22] To improve the photoelectrochemical performance, it is necessary to increase electrons transference and to reduce charge recombination.

Studies show that the presence of metallic nanoparticles (NPs) on semiconductor surface can improve the photocurrent intensity.[23] Liu *et al.*[24] investigated the surface plasmon resonance (SPR) function of silver nanoparticles on WO_3/Ag/CdS films for photoelectrochemical water splitting. This structure exhibited high photoelectrocatalytic performance in comparison to that of pristine WO_3 material. Similarly, Hu *et al.*[25] reported a simple method to prepare Au/WO_3 composite photoanodes for solar water oxidation. Further, the authors reported that in presence of Au nanoparticles, the photocurrent was improved by more than 80% at low potentials (<0.6 V vs. SCE). However, in most cases, the use of semiconductors films modified with metals involved expensive techniques and apparatus. In this paper, we present in detail the preparation of WO_3 films by simple drop-casting method and its functionalization with silver or platinum NPs. We examined the optical, structural, and photoelectrochemical properties of these films, and investigated their photocatalytic activity for progesterone hormone degradation in aqueous solution under polychromatic irradiation in HP and EHP configurations.

Results and Discussion

Structural and Optical Characterization

The phase structure of the annealed films was examined by the XRD technique. Figure 1a show XRD patterns of WO_3 films and those of WO_3 powder, which was prepared from the same tungsten precursor (tungsten citrate after annealing process at 500 °C), for comparison. All the diffraction peaks are in good agreement with the monoclinic structure of WO_3 (ICSD N° 17003).[26]

For WO_3 powder, the apparent (0 0 2), (0 2 0), and (2 0 0) diffraction signals can be observed in 2θ equal to 23.14°, 23.61° and 24.37°, respectively. For the film samples, these signals were overlapped, suggesting that films are extremely and composed of very small WO_3 particles. For the annealing of WO_3 films, the XRD data indicated a preferential ground of (120) plane, while the ($\bar{1}$12) plane almost disappeared. Further, 2θ signals equivalent to 38.28°, 44.45° and 64.80° attributed to FTO-glass are observed for all film samples.[23] In addition, in Figure 1b, the diffraction peaks for the cubic structure of the metallic NPs of Ag and Pt on WO_3 films are observed (ICSD No. 53759 and ICSD No. 64921, respectively).[27,28]

The lattice parameters for the monoclinic WO_3 phase were determined by Rietveld refinement (Figure S1 and Figure S2 in the Supporting Information). Among the common crystal phase monoclinic WO_3 is the most stable phase at room temperature.[29,30]

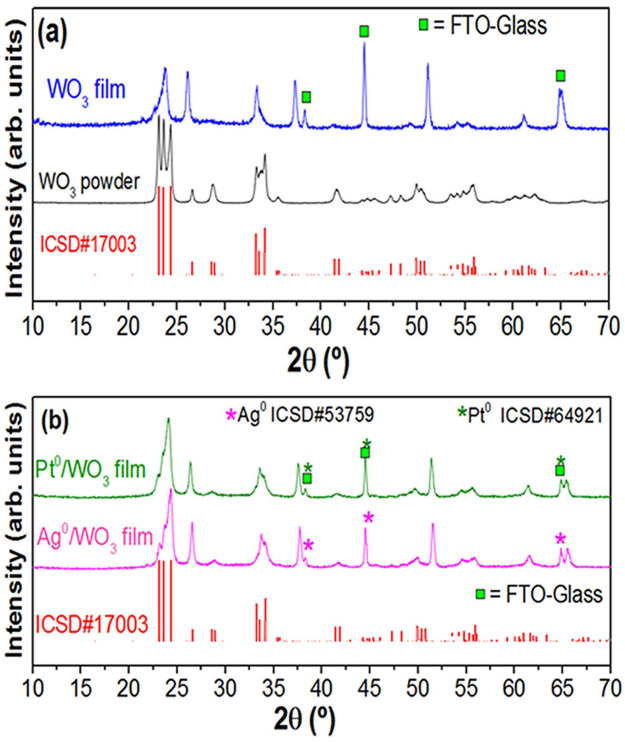

Figure 1. XRD pattern of bare and functionalized WO_3 film prepared by drop casting method and WO_3 powder with annealing at 500 °C for 2 h. Vertical bars indicate planes position and intensity of monoclinic WO_3 (ICSD No.17003).

The optical behavior of films was investigated by UV-Vis spectroscopy, and the results are shown in Figure 2. Figure 2a shows that the films had a maximum transmittance of ~85% in the visible region. At wavelengths lower than 420 nm, light was absorbed, suggesting that electron transition may have occurred from the valence band to the conduction band by overcoming the band gap energy.

From these UV-Vis curves, the optical E_{BG} values could be estimated by employing the Tauc method, considering indirect allowed transitions.[31] The E_{BG} values were calculated from the plot of $(\alpha h\upsilon)^{1/2}$ versus $h\upsilon$, and the linear portion of the graphic was extrapolated to $(\alpha h\upsilon)^{1/2}$ equal to zero, intersecting the energy axis as shown in Figure 2b. Thus, optical E_{BG} values of 3.23, 3.20, and 3.15 eV were estimated for WO_3, Ag^0/WO_3, and Pt^0/WO_3films, respectively. These values are in good agreement with the values reported in literature for WO_3 films.[32] Owing to the presence of the metal particles, the E_{BG} decreases slightly, suggesting that presence of metal NPs on semiconductor oxide surface leads to greater absorption in the visible region. In addition, the absorption spectra show a small displacement in the absorption edges to superior wavelengths. In principle, the narrowing of E_{BG} in semiconductors occurs due to the presence of localized states between the VB and CB or sensitizer bound to the surface of the catalyst.[33] The small variation in the optical E_{BG} values suggests that the addition of Ag^0 and Pt^0 does not alter the pristine structure of the WO_3 films, as occurs in the semiconductor doping.[34,35] Besides, according to the literature, WO_3 powders have lower E_{BG} than WO_3 films.[32] Aiming to evaluate this question, the UV-Vis spectra in the reflectance mode was obtained for WO_3 powder, and optical E_{BG} was estimated at 2.59 eV (see Figure S3).

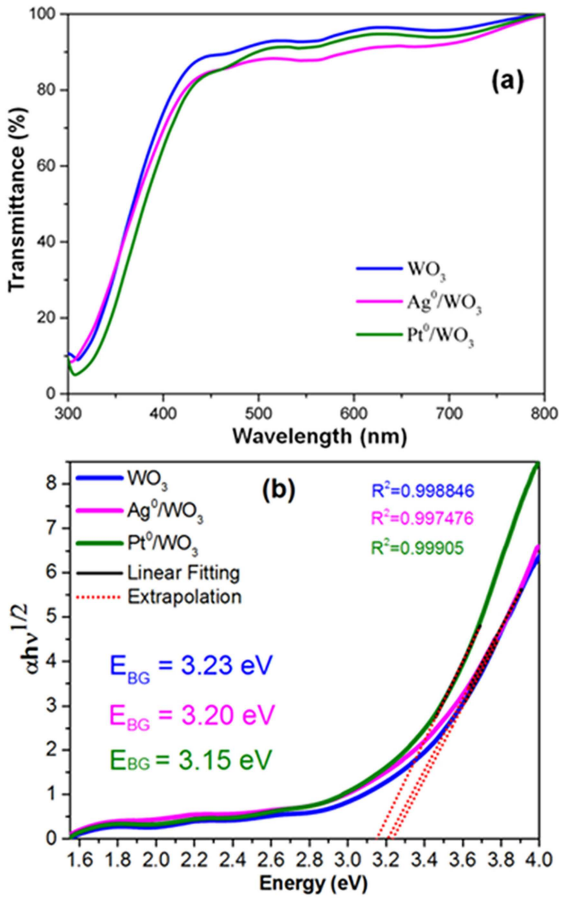

Figure 2. (a) UV-Vis transmittance curves for WO_3, Ag^0/WO_3 and Pt^0/WO_3 films; (b) Band gap energy estimated by Tauc method.

Morphological Characterization

After two layers were deposited and annealed at 500 °C, the WO_3 films had an approximate particle density of 3.1 ± 0.6 mg cm^{-2}. The morphological characterization of immobilized WO_3 particles on FTO-glass based on FE-SEM is presented in Figure 3.

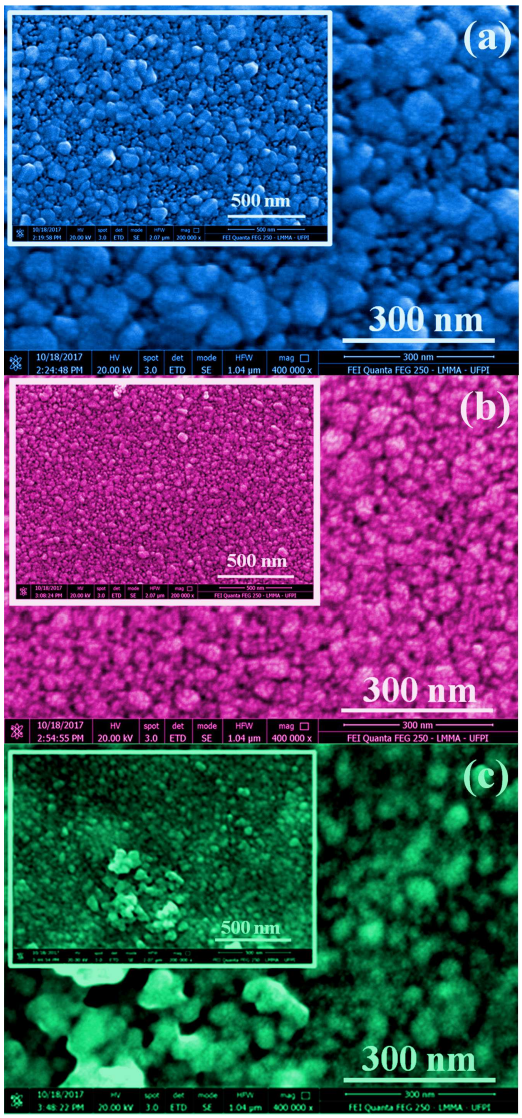

Figure 3. FE–SEM images of the surface (a) WO_3, (b) Ag^0/WO_3 and (c) Pt^0/WO_3 films. Inset: high magnification image of the surface. The larger image has a linear scale bar 300 nm in size and the smaller image has a linear scale bar with a size of 500 nm.

All films present similar morphology, and they comprise slightly spherical particles of size 50—80 nm and irregular shapes. However, these particles seem be formed by agglomeration with other smaller particles. The FE-SEM images in Figure 3a (WO_3 film) reveal nanoparticles with form analogous to crystals, as expected for the monoclinic structure of WO_3.[36] However, no noticeable evidence of metal NPs was observed on the modified WO_3 films shown in Figure 3a and Figure 3b, probably owing to the small size of metal particles.

Photoelectrochemical Investigation

Photoelectrochemical properties were investigated using a three-electrode setup under polychromatic irradiation. Figure 4 shows the cyclic voltammogram obtained in a potential window from 0.1 to 1.2 V. In the dark, only a small current was registered. To investigate the influence of number of WO_3 films layers on the photoelectrochemical response, WO_3 electrodes were fabricated with one, two, and three layers, and the results are shown in Figure 4a. The WO_3 electrode film with only one layer showed a photocurrent density slightly lower than that of the film with two layers. This is probably because the film with two layers is a better anchored semiconductor. Films prepared with three layers registered a decrease in photocurrent response possibly owing to an increase in FTO-glass resistance, which was attributed to three successive thermal treatment. WO_3 electrodes with two layers were functionalized with metallic nanoparticles by the photoreduction method. All photoelectrochemical examinations presented hereinafter were developed with the two-layered WO_3 electrode.

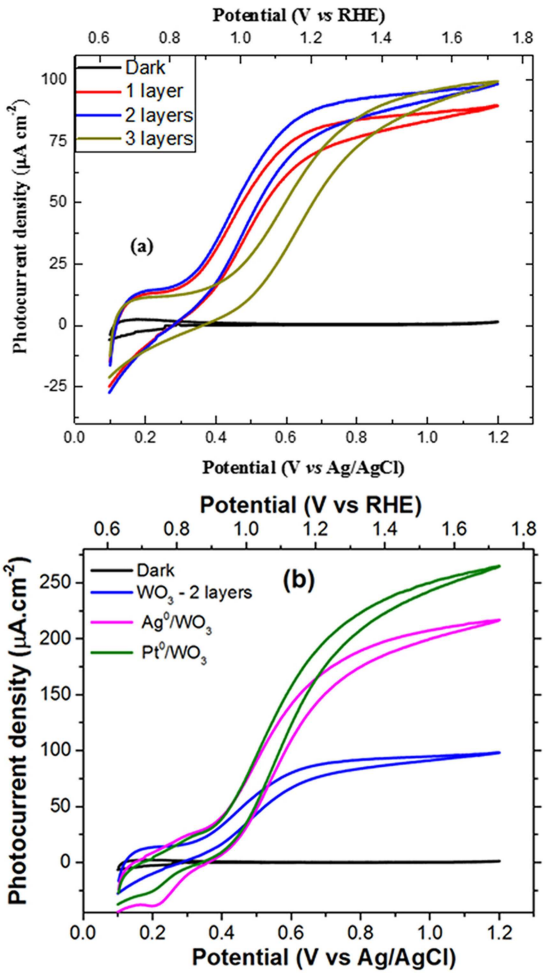

Figure 4. Photocurrent density (I) – voltage (V) curves with light on/off cycles, collected with a scan rate of 20 mV s^{-1} of (a) WO_3 electrode in different layers and (b) Functionalized with NPs.

Figure 4b shows the voltammograms for unmodified WO_3 for comparison with those of the WO_3 modified with Ag^0 and Pt^0 NPs. The presence of metal NPs on the WO_3 film surface clearly increased the photocurrent density by almost 2.5 times. At 0.8 V (vs. Ag/AgCl), the irradiated curves reached 190 and 225 μA cm^{-2} for Ag^0/WO_3 and Pt^0/WO_3, respectively. In principle, the current response can be attributed to the electron/hole (e^-/h^+) charge separation process. In *n*-type semiconductors, charges separation occurs under light irradiation with $h\nu \geq E_{BG}$. If the reaction kinetics of the hole with any species present in the solution is faster than the process of electron-hole recombination, the photogenerated electrons can be transferred through the crystallites that constitute the film.[37] Meanwhile, the electron can reach the conductive substrate and be collected for the external circuit.[38,39] A current gain was observed for both functionalized films probably owing to the interaction of WO_3 particles with metals NPs. Valenti *et al.*[40] reported the enhancement of the photoelectrochemical performance using a $CuWO_4$ film modified by Au nanoparticle as electrode; this enhancement was attributed to a combination of effects such as plasmon resonance energy transfer (PRET), hot electron injection, and light scattering. Thus, the increase in current occurs because the metals NPs act as electron traps or as light scattering centers. However, recently our study group showed the occurrence of electrons-holes charges recombination, even under the bias of the semiconductor.[23]

Photocurrent behaviors were registered using linear sweep voltammograms for electrodes annealed at 500 °C with interrupted light (chopper in 0.2 Hz). The results are shown in Figure 5a–c.

As discussed earlier, in general, the addition of metallic particles on the film surface more than doubled the photocurrent. The Pt^0/WO_3 electrode exhibited the highest photocurrent density of 250 μA cm^{-2} at 1.2 V vs. Ag/AgCl. From these line sweep curves, the flat band potential (E_{fb}), which is considered an approximation of the potential of the Fermi level, could be estimated. It is important to determine the E_{fb} of a semiconductor before its application in any photoelectrochemical proposition.[41,42] Here, the E_{fb} values were determined using a similar methodology to that used by Costa and co-works[23] they employed the Burter–Gärtner model (i.e., the variation of the square of the current). The E_{fb} values are equal for all electrodes of WO_3 (here ~0.34 V *vs* Ag/AgCl), suggesting that no structural modification or doping occurred in semiconductor lattice because of its modification with Ag^0 and Pt^0 NPs.

From E_{BG} and E_{fb} values, the relative positions of the edges of the conduction and valence bands of the semiconductor can

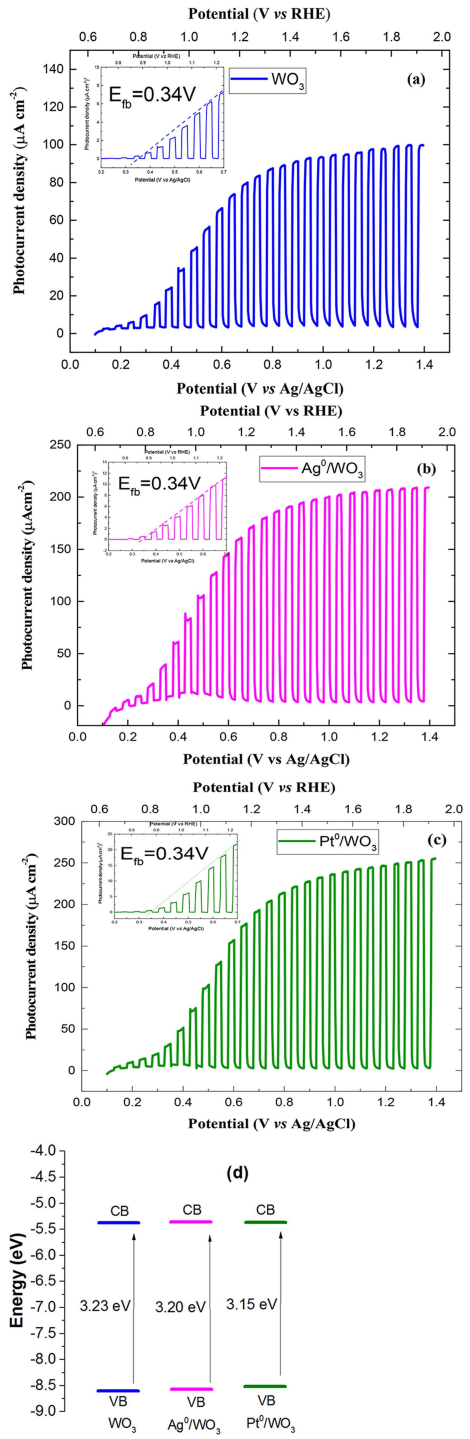

Figure 5. Linear sweep voltammetry curves of (a)WO_3, (b)Ag^0/WO_3 and (c) Pt^0/WO_3 illuminated with chopped visible light in an 0.1 mol L^{-1} Na_2SO_4 aqueous solution and (d)Valence (VB) and conduction (CB) band potentials for bare and functionalized WO_3 films. Inset: J^2 *vs* V curves by Butler-Gärtner Model.

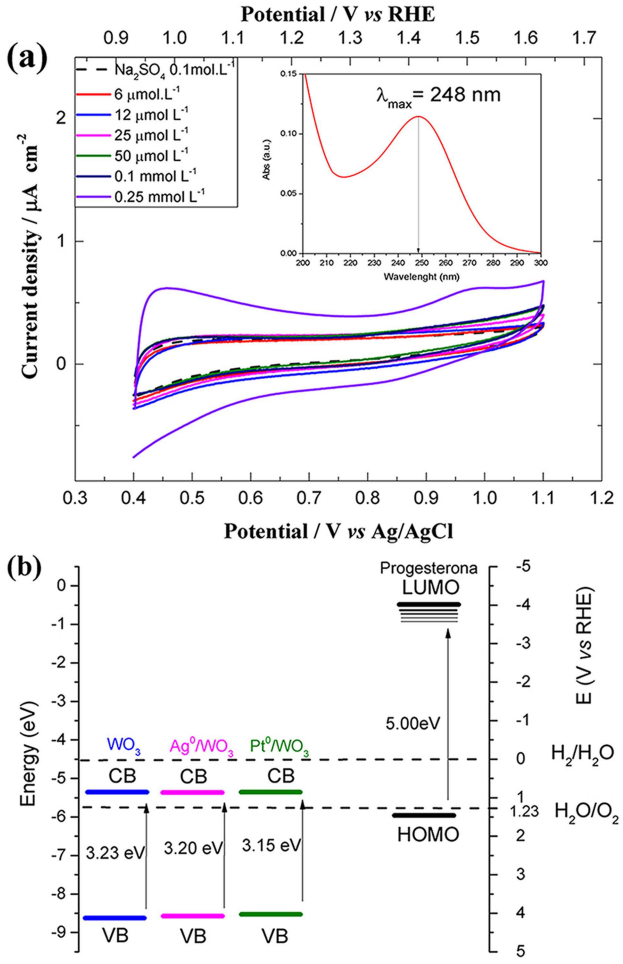

Figure 6. (a) Cyclic voltammograms (20 mV s^{-1}) for WO_3 electrode in the dark, in 0.1 mol L^{-1} Na_2SO_4 aqueous solution and in supporting electrolyte containing different concentration for progesterone and (b) Energy diagram for the semiconductor/progesterone hormone interface in aqueous solution, considering the highest occupied and the lowest unoccupied molecular orbitals, as well as the valence and conduction band edges for WO_3 electrodes.

be estimated using equations 1 and 2 shown in the Experimental Section. These positions are shown in Figure 5d.

Figure 6 presents the cyclic voltammogram for progesterone and the energy diagram for the semiconductor/progesterone hormone interface in aqueous solution. Figure 6a shows voltammograms in the dark (20 mV s^{-1}) obtained in solutions with different concentrations of progesterone in a supporting electrolyte (10 mL). For a potential range of 0.4 to 1.1 V (vs. Ag/AgCl), an oxidation peak current was observed with an onset potential of 0.8 V and the maximum peak for 0.97 V for the solution with 0.25 mmol L^{-1} progesterone. To make sure that this signal is related to progesterone, voltammograms were obtained for more diluted solutions. The solution was gradually diluted in the supporting electrolyte until the extinction of the peak. The potential for progesterone oxidation was converted into the energy scale by employing equations 1 and 2 as −6.0 eV. For organic compounds, this maximum oxidation energy value can be attributed to the highest occupied molecular orbital (HOMO) level. From the absorption UV-Vis curve presented in the inset in Figure 6a for progesterone, the gap energy between HOMO and LUMO of the pollutant was estimated.

The progesterone UV-Vis absorption spectrum exhibited a unique absorption band at 248 nm. Considering [E(eV) = 1241/λ(nm)], the corresponding energy value is 5.0 eV. Thus, for this value for the gap energy in progesterone, the LUMO energy level corresponds to −1.0 eV. Knowledge of the relative positions of E_{fb} and the oxidation potential of the pollutant allows estimation of the possible successful application of the semiconductor for photocatalytic degradation. The energy diagram for the semiconductor and hormone are shown in Figure 6b. The diagram presents the relative position of conduction, and the valence band edges are favorable for the oxidation of progesterone as the valence band edge has a more positive potential than the HOMO level of the pollutant. Thus, the photogenerated holes in the valence band oxidize the progesterone. In addition, in modified WO_3 with Ag^0 or Pt^0 NPs, the photoinduced charge separation should be improved as these metal NPs trap the electrons, thereby reducing recombination of the charges.

Progesterone Degradation

The photocatalytic activity of WO_3, Ag^0/WO_3, and Pt^0/WO_3 films for the degradation of progesterone hormone in aqueous medium was investigated using systems in heterogeneous photocatalysis (HP) and electrochemically assisted heterogeneous photocatalysis (EHP) configurations. Figure 7 shows the degradation efficiency of the progesterone aqueous solution under polychromatic irradiation, reuse of semiconductors, kinetics of degradation, and a schematic mechanism proposed to explain the improvement in charge separation by metal NPs during the photocatalytic process.

As shown in Figure 7a, the first step is the adsorption process on the photocatalyst surface for 30 min because the system is not illuminated. After irradiation, the hormone concentration decreased with time because of the formation of the oxidizing species photogenerated in the system.[43] The degradation efficiency of the progesterone hormone irradiated by photolysis was only 2.8% after 3 h under irradiation (Table 1). However, in the HP and EHP configurations, the efficiency reached the highest values, especially so in the EHP configuration. In HP configuration, WO_3, Ag^0/WO_3, and Pt^0/WO_3 photocatalysts exhibited an increase in degradation efficiency of 6.4%, 6.8%, and 7.0%, respectively, for the same illumination time. For the EHP configuration, WO_3, Ag^0/WO_3, and Pt^0/WO_3 photocatalysts realize degradation more efficient by 21.6%, 22.6%, and 26.7%, respectively.

In comparison to the WO_3 films, the metal NPs improved progesterone degradation in both configurations. After irradiation, the photoexcited electrons for the conduction band were trapped by the metallic NPs, inhibiting electron-hole recombination.[44] In addition, surface plasmon resonance and light scattering promoted by Ag^0 and Pt^0 NPs onto WO_3 films improved the photocatalytic activity.[45]

In EHP configuration, the electrodes are polarized under potential. Thus, for the *n*-type semiconductor, when irradiated, the electrons are driven toward the conductor substrate,

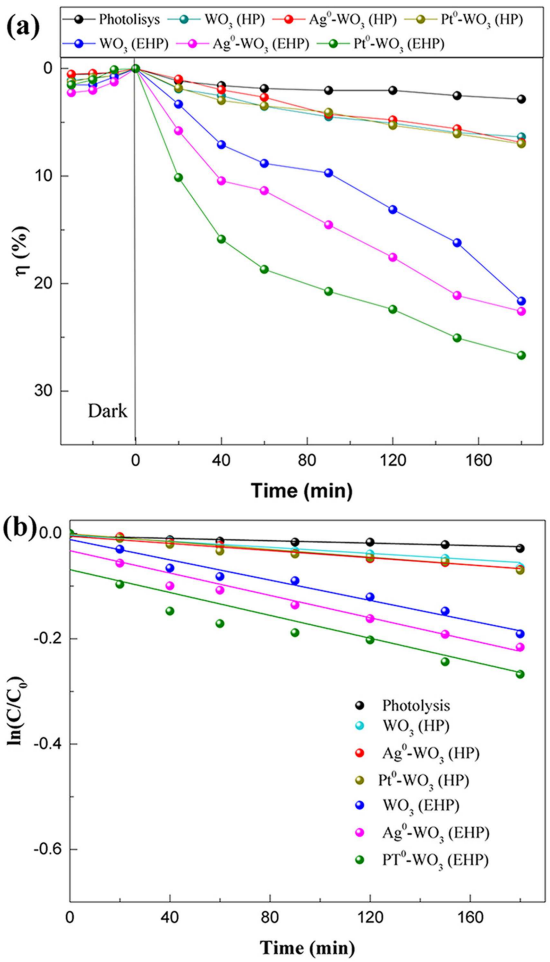

Figure 7. (a) Degradation efficiency of progesterone aqueous solution under polychromatic irradiation at (24 ± 2) °C by photolysis, heterogeneous photocatalysis (HP) and electro-assisted HP (EHP) using WO_3, Ag^0/WO_3 and Pt^0/WO_3 electrodes, (b) Kinetics of degradation, (c) reusability of the (•) WO_3, (•) Ag^0/WO_3 and (•) Pt^0/WO_3 electrodes in the EHP system for progesterone degradation under irradiation of visible light and (d) Schematic illustration of the mechanism of charge separation and photocatalytic process over photocatalyst under irradiation of visible light.

Table 1. Catalytic efficiency and degradation kinetic of the progesterone in different systems.

Catalytic System	Photocatalyst Film	Catalytic Efficiency η [%]	Degradation Kinetic *k* [min^{-1}]
Photolysis	–	2.8	1.12×10^{-4}
HP	WO_3	6.4	2.88×10^{-4}
EHP		21.6	9.62×10^{-4}
HP	Ag^0/WO_3	6.8	3.41×10^{-4}
EHP		22.6	10.61×10^{-4}
HP	Pt^0/WO_3	7.0	3.67×10^{-4}
EHP		26.7	10.86×10^{-4}

enhancing charge separation. Further, Oliveira *et al.*[16] reported better results for TiO_2 and TiO_2/WO_3 electrodes in the EHP configuration in the photocatalytic remediation of 17-α-ethinylestradiol in aqueous solution. The advantage of using the EHP technique is that it realizes faster degradation and is also inexpensive.[46] Some strategies to remove progesterone from

water, such as photolysis by UVA light[47] and oxidation with potassium permanganate in wastewater effluents[48], were reported in the literature, but electrochemically assisted photodegradation with WO_3 films has not yet been reported, to the best of our knowledge.

As observed in Figure 7b, the degradation of progesterone in aqueous solution can be adjusted by pseudo-first-order kinetics.[49] The photocatalytic rates were calculated using the equation,[10] $\ln\left(\frac{A_t}{A_0}\right) = -kt$, where k is a degradation rate constant of progesterone hormone (min^{-1}), and t is the irradiation time (min). Thus, the progesterone photodegradation was fitted to a plot of ln (A_t/A_0) vs time to obtain the rate constant (Figure 7b). The k value for progesterone removal is 1.12×10^{-4} min^{-1} in photolysis, using the WO_3 electrode in the HP and EHP systems correspond to 2.88×10^{-4} min^{-1} and 9.62×10^{-4} min^{-1}, respectively. Upon functionalization, slightly higher values were obtained for Ag^0/WO_3 and Pt^0/WO_3: 3.41×10^{-4} and 3.67×10^{-4} min^{-1}, respectively, for HP configuration and 10.61×10^{-4} $min^{-1}$and 10.86×10^{-4} min^{-1}, respectively, in the EHP configuration. All chemical contaminants degradation curves obey a pseudo-first-order kinetics reaction. In general, the efficiency of photodegradation of hormones depends on many factors such as the efficiency of photodegradation of estrogenic steroidal hormones, physicochemical properties and initial concentrations of the pollutants, light source, photon flux, type, catalyst loading, pH, and temperature.[50] Progesterone has relatively low water solubility and is reasonably hydrophobic. As the progesterone solubility limit in water is quite low, ~8.81 mg L^{-1} (at 25°C),[51] the examinations could not be performed using progesterone solutions with higher concentrations. As discussed before, hormones can be considered a persistent pollutant, and these results revealed that the progesterone in water is not easily degraded only by photolysis.

A comparison of the results for the HP configuration shows that the WO_3 films functionalized with Ag^0 and Pt^0 NPs had slightly better performance than the WO_3 film. A comparison of all electrodes in the EHP configuration showed that the Pt^0/WO_3 electrode exhibited the highest efficiency for progesterone degradation. According to literature, Pt^0NPs act as one of the most efficient charge transfer facilitators.[23,52,53] The photocatalytic activities of WO_3 modified by Ag^0 NPs are very sensitive to metal sizes and form.[54] Employing the surface plasmon resonance is an efficient method to localize photon absorption at the semiconductor surface by incorporating plasmonic metal NPs on the semiconductor electrode. The plasmon resonance frequency and intensity depends on the geometry and distribution engineering of the NPs and the dielectric property of the surrounding medium.[55] In this study, the highest performance for progesterone degradation (~27%) was observed for the Pt^0/WO_3 electrode in the EHP configuration. These results can be considered promising, considering progesterone is a neutral molecule and is difficult to degrade. Thus, it can be concluded that the EHP configuration is more suitable as compared to the HP configuration and photolysis in polychromatic light for degrading progesterone in aqueous solution.

The reusability of the primitive and functionalized WO_3 catalysts electrodes in the EHP configuration for progesterone degradation was evaluated (Figure 7c). The results show that the WO_3 decreased the photocurrent values in each cycle, probably because the electrode can suffer photocorrosion during five cycles of utilization. Further, the results suggest that functionalized WO_3 electrodes were more stable, with emphasis on the Pt^0/WO_3 electrode. In general, there is a small decrease in catalytic activity after five successive catalytic cycles with efficiencies of 15.6%, 18.64%, and 21.43%, for WO_3, Ag/WO_3, and Pt/WO_3 electrodes, respectively. Figure 7d shows the mechanism of photogenerated e^-/h^+ pair separation. This indicates that more generated charge carriers participate in the photoelectrochemical reaction because of the interface with metal NPs for generating reactive $^{\bullet}OH$ and other species for degrading progesterone.

Therefore, the results presented here indicate that the WO_3 film presents reasonable morphological, structural, and optical properties that are improved when the structure is modified by functionalization with metallic NPs. However, improvement of the photoelectrochemical performance of WO_3 for photocatalytic organic pollutant degradation in drinking water, such as progesterone, is attributed to the efficiency of transmission of the photogenerated charges, enhanced light absorption, and reduction in the photogenerated e^-/h^+ recombination rate.

Conclusion

In summary, this work reveals that WO_3 films can successfully be synthetized by the drop-casting method at 500 °C for 2 h and functionalized with Ag^0 and Pt^0 NPs by photoreduction. All films prepared exhibit monoclinic structure, irregular spherical morphology, and the decrease of indirect optical EBG (calculated by Tauc method). Photoelectrochemical analyzes indicate that the functionalization with metallic NPs accelerates the electron transport and increases the separation of the electrons and photogenerated holes, thus reducing the recombination time of the e^-/h^+ pair. Consequently, the oxidative degradation of progesterone in aqueous solution under polychromatic irradiation was tested in the HP and EHP configurations using WO_3, Ag^0/WO_3, and Pt^0/WO_3 electrodes as a photocatalyst for 3 h. When the photoanode was biased at +0.7 V vs Ag/AgCl, the photocatalytic efficiency improved because the applied potential suppressed charge recombination. Thus, the highest photocatalytic activity was obtained for the EHP configuration for the Pt^0/WO_3 electrode; in addition, the functionalized electrodes films have higher stability as they could be used five times with lower loss photocurrent and enhanced photooxidation of the hormone. Therefore, WO_3 films functionalized with NPs are promising candidate photoanode material and with the EHP configuration can provide direction to more studies on potential applications of PEC water splitting and photodegradation of organic pollutants.

Experimental Section

Preparation of WO_3, Ag^0/WO_3, and Pt^0/WO_3 Films

Tungsten citrate was synthesized by the polymeric precursor method.[56] Tungstic acid (H_2WO_4; 99.0% purity, Aldrich), ethylene glycol or ethane-1,2-diol ($C_2H_6O_2$; 99.5% purity, Contemporary Chemistry Dynamics LTDA), and citric acid ($C_6H_8O_7$; 99.5% purity, Sigma-Aldrich) were used as raw materials. The preparation stages were as follows: (I) Dissolution of 3×10^{-2} mol$C_6H_8O_7$ in deionized water (DI-H_2O) at room temperature for 10 min; (II) dissolution of 1×10^{-2} mol H_2WO_4 into aqueous solution of $C_6H_8O_7$ at 85 °C for 5 h under constant stirring to allow the homogenization and formation of tungsten citrate solution using 200 drops of ammonium hydroxide solution ($NH_3.H_2O$; 30.0% purity, Contemporary Chemistry Dynamics LTDA); and (III) after homogenization of the tungsten citrate solution, the gravimetric procedure was performed using five crucibles in order to find the precise molar concentration (grams of tungsten citrate/mol of WO_3).

WO_3 films electrodes were prepared on fluorine-doped tin oxide (FTO, Aldrich, surface resistivity: 7 Ω/sq) of dimensions 1.0×2.5 cm^2, which was previously cleaned by sonication with deionized water, neutral liquid soap, and isopropyl alcohol in successive steps for 15 min, respectively. After this procedure, some drops of tungsten citrate were scattered evenly on the substrate of the FTO-glass. After drying naturally ~10 min, the films were heated (2 °C/min) and maintained at 500 °C for 120 min in a furnace. To form a second layer, tungsten citrate was dropped again, and the thermal treatment was repeated. The surface films were modified with silver (Ag^0) or platinum (Pt^0) in aqueous solution of silver nitrate ($AgNO_3$, 1.0×10^{-3} mol L^{-1}) or hexachloroplatinic acid hexahydrated ($H_2PtCl_6.6H_2O$, 1.0×10^{-3} mol L^{-1}), respectively. WO_3 films were immersed in the Ag^+ and Pt^{4+} precursor solutions in a beaker glass for 10 s. Then, the WO_3 films were subjected to UV irradiation in a closed box with three STARLUX® 20 W lamps. The films were placed at approximately 40 cm from the UV source for a period of 5 min. Thereafter, the films were washed several times with deionized water to guarantee complete removal of the ions.

Structural and Optical Characterization of the Ohotoelectrodes

X-ray diffraction (XRD) patterns of the WO_3, Ag^0/WO_3 and Pt0/WO_3 films were obtained using a LabX XRD-6000diffractometer (Shimadzu, Japan) with Cu-Kα radiation (λ = 0.15406 nm) in the 2θ range of10° to 70° with a scanning velocity of 1° min^{-1}. The diffraction patterns were compared to the data from the Inorganic Crystal Structure Database (ICSD). The optical properties of the samples were recorded by a Shimadzu UV-2600 spectrophotometer equipped with an integrating sphere using barium sulfate as a reference standard. The semiconductor band gap energy was estimated by Tauc method from the UV-Vis curves.[57]

Morphological Characterization and Photoelectrochemical Measurements

The morphology of the samples was characterized by field emission-scanning electron microscopy (FE-SEM, FEI Quanta FEG 250). The images were obtained with a working voltage of 20 kV. The photoelectrochemical properties were investigated using an electrochemical cell produced with an optic glass window (100% transmittance for λ > 360 nm). Working electrodes were the primitive or functionalized WO_3 films (with geometrical area of 1 cm^2); a Pt wire was the counter electrode, and Ag/AgCl (in 3.0 mol L^{-1} KCl saturated aqueous solution) was the reference electrode (in Luggin capillary). A three-electrode system configuration was used, and Na_2SO_4 0.1 mol L^{-1} (pH 5.6) aqueous solution was employed as the inert support electrolyte. Measurements analyses were developed in a galvanostat/potentiostat (AutolabPGSTAT 302-N) in darkness and under polychromatic irradiation. A metallic vapor discharge lamp (HQI-TS NDL) with a nominal potency of 150 W was utilized to irradiate the WO_3 films for electrochemical and photoelectrocatalytic examination during the degradation of progesterone.

Photocurrent was measured using the cyclic voltammogram with a scan rate of 20 mVs^{-1} (in the dark and under irradiation). The flat band potential (Efb) was determined using the Butler-Gärtner model[58] based on linear sweep voltammetry (LSV) with the data recorded in the anodic potential range 0.1–1.2 V at a scan rate of 5.0 $mV s^{-1}$ using chopped illumination at 0.2 Hz. Chronoamperometric curves were registered under dark or light conditions with the electrodes polarized at +0.7 V (vs Ag/AgCl).

For comparison, the potential registered using the Ag/AgCl reference electrode was adjusted to a reversible hydrogen electrode (RHE), according to the equation:[16,59,60]

$$E\ (vs.\ \mathrm{RHE}) = E\ (vs.\ \mathrm{Ag/AgCl}) + 0.0591\ \mathrm{V} \times \mathrm{pH} + 0.199\ \mathrm{V} \quad (1)$$

Further, the potentials after adjustment with respect to the RHE (in volts) were converted to electron-volts (eV) using equation:[61]

$$\mathrm{E(eV)} = [-4.5\ \mathrm{eV} - \mathrm{eE_{(RHE)}}] \quad (2)$$

Progesterone Degradation Studies

The photocatalytic activity of WO_3, Ag/WO_3, and Pt/WO_3 film electrodes was investigated using a progesterone solution with an initial concentration (C_0) of 0.35 mg L^{-1}dissolved in Na_2SO_4 0.1 mol L^{-1} aqueous solution as the supporting electrolyte (pH 5.6). In this investigation, three configurations were considered: (i) photolysis by irradiation of 10 mL progesterone in the supporting electrolyte without the photocatalyst film, using only a clean FTO-glass; (ii) heterogeneous photocatalysis (HP) using a system with a photocatalyst film; and (iii) electrochemically assisted heterogeneous photocatalysis (EHP), which was carried out with photoelectrodes polarized in +0.7 V vs Ag/AgCl. In all configurations, the system was not heat or stirred. The kinetic investigation occurred in under conditions of darkness and irradiation for 3 h; aliquots were collected at different times and analyzed using the UV-vis spectrophotometer. The degradation efficiency (η) was calculated according to the following equation:[62] $\eta = \frac{A_0 - A_t}{A_0} x\ 100$, where A_0 is the initial absorbance, and A_t is the absorbance of progesterone hormone after irradiation time "t.".

Acknowledgements

This study was supported by the Brazilian research financing institutions: CNPq (479644/2012-8, 312318/2017-0 and 304531/2013-8), FAPESP (2013/07296-2), and CAPES.

Conflict of Interest

The authors declare no conflict of interest.

Keywords: nanoparticles · photodegradation · progesterone · thin films · tungsten trioxide

[1] S. V. Mohite, V. V. Ganbavle, K. Y. Rajpure, *J. Energy Chem.* **2017**, *26*, 440-447.
[2] I. A. Mkhalid, *Ceram. Int.* **2016**, *42*,15975–15980.
[3] J. O. Ojoghoro, A. J. Chaudhary, P. Campo, J. P. Sumpter, M. D. Scrimshaw, *Sci. Total Environ.* **2017**, *579*, 1876–1884.
[4] P. Avar, G. Maasz, P. Takács, S. Lovas, Z. Zrinyi, R. Svigruha, A. Takátsy, L. G. Tóth, Z. Pirger, *Drug Test. Analysis* **2016**, *8*, 123–7.
[5] D. Nasuhoglu, D. Berk, V. Yargeau, *Chem. Eng. J.* **2012**, *185-186*, 52-60.
[6] E. Touraud, B. Roig, J. P. Sumpter, C. Coetsier, *Int. J. Hyg. Environ. Health*, **2011**, *214*, 437–441.
[7] G. R. Tetreault, C. J. Bennett, K. Shires, B. Knight, M. R. Servos, M. E. McMaster, *Aquat. Toxicol.* **2011**, *104*, 278–290.
[8] R. Andreozzi, V. Caprio, A. Insola, R. Marotta, *Catal. Today* **1999**, *53*, 51–59.
[9] K. G. Linden, M. Mohseni, *Comprehensive Water Quality and Purification* **2014**, *2*, 148–172.
[10] Y. M. Hunge, M. A. Mahadik A. V. Moholkar, C. H. Bhosale, *Ultrason. Sonochem.* **2017**, *35*, 233–242.
[11] R. Daghrir, P. Drogui, D. Robert, *J. Photochem. Photobiol. A* **2012**, *238*, 41–52.
[12] S. V. Mohite, V. V. Ganbavle, K. Y. Rajpure, *J. Photochem. Photobiol. A* **2017**, *344*, 56–63.
[13] D. Wang, P. S. Bassi, H. Qi, X. Zhao, Gurudayal, L. H. Wong, R. Xu, T. Sritharan, Z. Chen, *Mater.* **2016**, *9*, 348–13.
[14] R. R. Kharadea, S. S. Malib, S. P. Patil, K. R. Patil, M. G. Gang, P. S. Patil, J. H. Kim, P. N. Bhosale, *Electrochim. Acta.* **2013**, *102*, 358–368.
[15] E. H. Umukoro, M. G. Peleyeju, J. C. Ngila, O. A. Arotiba, *Chem. Eng. J.* **2017**, *317*, 290–301.
[16] H. G. Oliveira, L. H. Ferreira, R. Bertazzoli, C. Longo, *Water Res.* **2015**, *72*, 305–314.
[17] J. Y. Zheng, Z. Haider, K. T. Van, A. U. Pawar, M. J. Kang, C. W. Kim, Y.S. Kang, *CrystEngComm* **2015**, *17*, 6070–6093.
[18] S. Walia, S. Balendhran, H. Nili, S. Zhuiykov. G. Rosengarten. Q. H. Wang, M. Bhaskaran, S. Sriram, M. S. Strano, K. Kalantar-Zadeh, *Prog. Mater. Sci.* **2013**, *58*, 1443–1489.
[19] I. M. Szilágyi, B. Fórizs, O. Rosseler, A. Szegedi, P. Németh, P. Király, G. Tárkányi, B. Vajna, K. V. Josepovits, K. László, A. L. Tóth, P. Baranyai, M. Leskelä, *J. Catal.* **2012**, *294*, 119–127.
[20] S. V. Mohite, V. V. Ganbavle, K. Y. Rajpure, *J. Alloys Compd.* **2016**, *655*, 106–113.
[21] P. A. Shinde, V. C. Lokhande, N. R. Chodankar, T. Ji, J. H. Kim, C. D. Lokhande, *J. Colloid Interface Sci.* **2016**, *483*, 261–276.
[22] K H. Ng, L. J. Minggu, W. F. Mark-Lee, K. Ariffin, M. H. H. Jumali, M. B. Kassim, *Mater. Res. Bull.* **2018**, *98*, 47–52.
[23] M. J. S. Costa, G. S. Costa, A. E. B. Lima, G. E. Luz Jr., E. Longo, L. S. Cavalcante, R. S. Santos, *Ionics* **2018**, *24*, 3291-3297.
[24] Z. Liu, J. Wu, J. Zhang, *Int. J. Hydrogen Energy* **2016**, *41*, 20529–20535.
[25] D. Hu, P. Diao, D. Xu, Q. Wu, *Nano Res.* **2016**, *9*, 1735–1751.
[26] S. Tanisaki, *J. Phys. Soc. Jpn.* **1960**, *15*, 573–581.
[27] L. Vegard. IX, *Philos. Mag. Ser.* **1916**, *31*, 83–87.
[28] H. Kahler, *Phys. Verh.* **1921**, *18*, 210.
[29] J. Y. Zheng, G. Song, J. Hong, K. V. Thanh, A. U. Pawar, D. Y. Kim, C. W. Kim, Z. Haider, Y. S. Kang, *Cryst. Growth Des.* **2014**, *14*, 6057–6066.
[30] J. H. Kim, B. J. Lee, P. Wang, M. H. Son, J. S. Lee, *Appl. Catal. A.* **2016**, *521*, 233–239.
[31] B. D. Viezbicke, S. Patel, B. E. Davis, D. P. Birnie, *Phys. Status Solidi B.* **2015**, *252*, 1700–1710.
[32] D. Valerini, S. Hernández, F. Di Benedetto, N. Russo, G. Saracco, A. Rizzo, *Mater. Sci. Semicond. Process.* **2016**, *42*, 150–154.
[33] L. Wang, J. Fan, Z. Cao, Y. Zheng, Z. Yao, G. Shao, J. Hu, *Chem. Asian J.* **2014**, *9*, 1904–1912.
[34] L. Wang, X. Zhang, H. Gao, J. Hu, J. Mao, C. Liang, P. Zhang, G. Shao, *Sci. Adv. Mater.* **2016**, *8*, 1256–1262.
[35] Q. Wang, J. Fan, S. Zhang, Y. Yun, J. Zhang, P. Zhang, J. Hu, L. Wang, G. Shao, *RSC Adv.* **2017**, *7*, 54662–54667.
[36] G. H. Go, P. S. Shinde, C. H. Doh, W. J. Lee, *Mater. Des.* **2016**, *90* 1005–1009.
[37] H. Yoon, M. G. Mali, M. Kim, S. S. Al-Deyab, S. S. Yoon, *Catal. Today.* **2016**, *260*, 89–94.
[38] S. Soedergren, A. Hagfeldt, J. Olsson, S.-E. Lindquist , *J. Phys. Chem.* **1994**, *98*, 5552–5556.
[39] A. Hagfeldt, M. Grätzel, *Chem. Rev.* **1995**, *95*, 49–68.
[40] M. Valenti, D. Dolat, G. Biskos, A. Schmidt-Ott, W. A. Smith, *J. Phys. Chem. C.* **2015**, *19*, 2096–2104.
[41] T. Bak, J. Nowotny, M. Rekas, C. C. Sorrell, *Int. J. Hydrog. Energy.* **2002**, 27, 991–1021.
[42] Y. Liu, J. Li, W. Li, H. He, Y. Yang, Y. Li, Q. Chen, *Electrochim. Acta.* **2016**, *210*, 251–260.
[43] K. M. Lee, C. W. Lai, K. S. Ngai, J. C. Juan, *Water Res.* **2016**, *88*, 428–448.
[44] M. A. Gondal, M. A. Suliman, M. A. Dastageer, G. K. Chuah, C. Basheer, D. Yang, A. Suwaiyan, *J. Mol. Catal. A: Chem.* **2016**, *425*, 208–216.
[45] J. Li, S. K. Cushing, D. Chu, P. Zheng, J. Bright, C. Castle, A. Manivannan, N. Wu, *J. Mater. Res.* **2016**, *11*, 1608–1615.
[46] K. Vinodgopal, P. V. Kamat, *Sol. Energy Mater. Sol. Cells* **1995**, *38*, 401–410.
[47] J. M. Jones, T. Borch, R. B. Young, J. G. Davis, C. R. Simpson, American Water Resources Association, Vail, Colorado, **2007**.
[48] P. B. Fayad, A. Zamyadi, R. Broseus, M. Prévost, S. Sauvé, *Chem. Cent. J.* **2013**, *7*, 84.
[49] A. Samad, S. Ahsan, I. Tateishi, M. Furukawa, H. Katsumata, T. Suzuki, S. Kaneco, *Chin. J. Chem. Eng.* **2018**, *26*, 529–533.
[50] K. Sornalingam, A. McDonagh, J. L. Zhou, *Sci. Total Environ.* **2016**, *550*, 209–224.
[51] S. H. Yalkowsky, Y. He, *J. Med. Chem.* **2003**, *46*, 4213–4213.
[52] N. M. Gupta, *Sust. Energ. Rev.* **2017**, *71*, 585–601.
[53] J. Kim, C. W. Lee, D. W. Choi, *Environ. Sci. Technol.* **2010**, *44*, 6849–6854.
[54] J. Ding, L. Zhang, Q. Liu, W.-L. Dai, G. Guan, *Appl. Catal. B.* **2017**, *203*, 335–342.
[55] Y. Liu, Z. Xu, M. Yin, H. Fan, W. C. L. Lu, Y. Song, J. Ma, X. Zhu, *Nanoscale Res. Lett.* **2015**, *10*, 374.
[56] L. S. Cavalcante, J. C. Sczancoski, V. C. Albarici, J. M. E. Matos, J. A. Varela, *Mater. Sci. Eng. B.* **2008**, *150*,18–25.
[57] M. Radecka, M. Rekas, A. Trenczek-Zajac, K. Zakrzewska, *J. Power Sources.* **2008**, *181*, 46–55.
[58] L. M. Pete in *Photoelectrochemical Solar Fuel Production* (Eds.: S. Giménez, J. Bisquert), Springer, *Cham*, **2016**, pp. 23.
[59] J. E. Yourey, B. M. Bartlett, *J. Mater. Chem.* **2011**, *21*, 7651–7660.
[60] A. E. B. Lima, M. J. S. Costa, R. S. Santos, N. C. Batista, L. S. Cavalcante, E. Longo, G. E. Luz Jr., *Electrochim. Acta.* **2017**, *256*, 139–145.
[61] A. J. Bard, L. R. Faulkner, *Electrochemical Methods: Fundamentals and Applications, 2nd ed.*, John Wiley & Sons, Inc., New York, **2000**, pp. 54.
[62] X. Wang, Z. Zhou, Z. Liang, Z. Zhuang, Y. Yu, *Appl. Surf. Sci.* **2017**, *423*, 225–235.

Manuscript received: October 19, 2018
Accepted manuscript online: November 21, 2018
Version of record online: ■■, ■■■